Reprinted from

APPLIED PHYSICS EXPRESS

Formation of Self-Assembled, Double-Perovskite, Ba_2YNbO_6 Nanocolumns and Their Contribution to Flux-Pinning and J_c in Nb-Doped $YBa_2Cu_3O_{7-\delta}$ Films

Sung Hun Wee, Amit Goyal, Yuri L. Zuev, Claudia Cantoni, V. Selvamanickam, and Eliot D. Specht

Appl. Phys. Express **3** (2010) 023101

© 2010 The Japan Society of Applied Physics

Person-to-person distribution (up to 10 persons) by the author only. Not permitted for publication for institutional repositories or on personal Web sites.

Applied Physics Express 3 (2010) 023101

Formation of Self-Assembled, Double-Perovskite, Ba_2YNbO_6 Nanocolumns and Their Contribution to Flux-Pinning and J_c in Nb-Doped $YBa_2Cu_3O_{7-\delta}$ Films

Sung Hun Wee[1,2], Amit Goyal[1], Yuri L. Zuev[1,3], Claudia Cantoni[1], V. Selvamanickam[4], and Eliot D. Specht[1]

[1] *Materials Science and Technology Division, Oak Ridge National Laboratory, Oak Ridge, TN 37831, U.S.A.*
[2] *Department of Materials Science and Engineering, University of Tennessee, Knoxville, TN 37996, U.S.A.*
[3] *Department of Physics, University of Tennessee, Knoxville, TN 37996, U.S.A.*
[4] *Department of Mechanical Engineering, University of Houston, Houston, TX 77204, U.S.A.*

Received December 12, 2009; accepted January 4, 2010; published online February 5, 2010

Ba_2RENbO_6 (RE = rare earth elements including Y) compounds are considered new additives for superior flux-pinning in $YBa_2Cu_3O_{7-\delta}$ (YBCO) films due to their excellent chemical inertness to and large lattice mismatches with YBCO. Simultaneous laser ablation of a YBCO target and a Nb metal foil attached to the surface of the target resulted in epitaxial growth of YBCO films having columnar defects comprised of self-aligned Ba_2YNbO_6 (BYNO) nanorods parallel to the *c*-axis of the film. Compared to pure YBCO, YBCO+BYNO films exhibited no T_c reduction as well as superior J_c performance with higher self- and in-field J_c by a factor of 1.5–7 and also exhibited a strong J_c peak for $H \parallel c$ indicative of strong *c*-axis correlated flux-pinning. © 2010 The Japan Society of Applied Physics

DOI: 10.1143/APEX.3.023101

High temperature superconducting (HTS) wires or coated conductors based on $REBa_2Cu_3O_{7-\delta}$ (RE = rare earth elements including Y, REBCO) films are capable of carrying high current without loss. This unique property enables fabrication of environmentally friendly electric power devices and smart electric grids with higher efficiency, smaller weight, footprints and/or sizes.[1] High critical current density, J_c, of REBCO films is essential not only to meet the required performance for these applications but also to lower manufacturing costs and ac losses of the wires. Recently, J_c performance in magnetic fields as well as at self-field has been remarkably increased via controlled introduction of non-superconducting nanometer scale defects into REBCO matrix.[2–12] In particular, creation of nanocolumnar arrays comprised of self-organized, non-superconducting nanodots/rods oriented along the *c*-axis with a controllable splay has resulted in a substantial improvement in the overall J_c over extensive fields and angular ranges as well as for the field parallel to the *c*-axis, $H \parallel c$.[5–12] So far, only very limited materials such as cubic-perovskite-structured, $BaMO_3$ (M = Zr and Sn) compositions that have ~6–8% lattice mismatches with REBCO materials have resulted in the formation of such columnar defects and enhanced flux-pinning. Hence, it is of great interest to find new flux-pinning additives that form self-assembled nanocolumns in REBCO films and which are more chemically inert with REBCO or are easier to incorporate into REBCO compared to the $BaMO_3$-type additives reported previously. Very recently, we have reported Ba_2RETaO_6 (BRETO) materials with cubic or distorted cubic double perovskite structures as a new class of additives that lead to superior flux-pinning and J_c in $YBa_2Cu_3O_{7-\delta}$ (YBCO) films.[13] These tantalates have excellent chemical inertness and large lattice mismatches (9–12%) with YBCO which result in phase separation and strain minimization driven self-assembly of BRETO nanocolumns in YBCO films.[14] Similar to these tantalates, rare earth barium niobates, Ba_2RENbO_6, which have an isotropic structure and similar lattice parameters to the tantalates, have also been reported to have excellent chemical inertness to YBCO.[15,16] It is also worthy of note that substitution of both Ta and Nb into the Cu site of YBCO is negligible due to greater thermodynamical stability of BRETO and BRENO compounds, compared to $YBa_2Cu_{3-x}Ta(\text{or Nb})_xO_{7-\delta}$.[17,18] Hence, these niobates are also excellent candidates as additives for formation of columnar defects and the related enhancement in flux-pinning of REBCO films.

In this work, we report on formation of columnar defects comprised of self-assembled Ba_2YNbO_6, (BYNO) nanorods in YBCO films and their contribution on flux-pinning and J_c. Although BYNO nanocolumns were formed by reaction between Nb and YBCO that involved small decomposition of YBCO, YBCO+BYNO films show massive improvement in flux-pinning and J_c without T_c degradation.

Nb-doped YBCO films were prepared by simultaneous laser ablation, using a KrF ($\lambda = 248$ nm) excimer laser, of a YBCO target and Nb foils with different widths affixed on the target. The samples were epitaxially grown on biaxially textured, IBAD-MgO templates with a $LaMnO_3$ cap layer that were supplied from Superpower, Inc. Detailed processing conditions were described in elsewhere.[10,13] The standard four-point probe method was used for the transport measurements including T_c and J_c with a voltage criterion of 1 μV/cm. Transmission electron microscopy (TEM) and scanning electron microscopy (SEM) were used for microstructural characterization.

Nb addition into YBCO films was found to result in formation of self-assembled BYNO nanocolumns within YBCO matrix. The volume fraction (%) of BYNO nanophase in Nb-doped samples increases with the addition of Nb as determined by detailed X-ray diffraction analysis and summarized in Table I. Nb doping level was controlled by varying the width of Nb foil attached on the YBCO target. Since laser ablation of the Nb foil produces a plume much smaller than that obtained from the YBCO target, the growth rate and consequently, the film thickness are proportionally reduced by increasing the Nb ablation area w.r.t. the total ablation area, for the same deposition time. Thicknesses of Nb-doped films with different volume fraction of BYNO nanocolumns were estimated via cross sectional TEM examination, as also summarized in Table I.

Figure 1 shows cross section TEM micrographs for a YBCO film containing 5.1% BYNO. As shown in Fig. 1(a), BYNO nanocolumns are formed through the entire film thickness and are primarily oriented along the *c*-axis of YBCO. The density of BYNO nanocolumns is estimated

 © 2010 The Japan Society of Applied Physics

Person-to-person distribution (up to 10 persons) by the author only. Not permitted for publication for institutional repositories or on personal Web sites.

Table I. XRD volume fraction (%) of BYNO nanophase and film thickness for Nb-doped YBCO films.

Nb foil width (mm)	Volume fraction of BYNO nanophase (%)	Film thickness (nm)
—	0	~800
4	0.3	~800
10	1.3	~650
20	5.1	~500

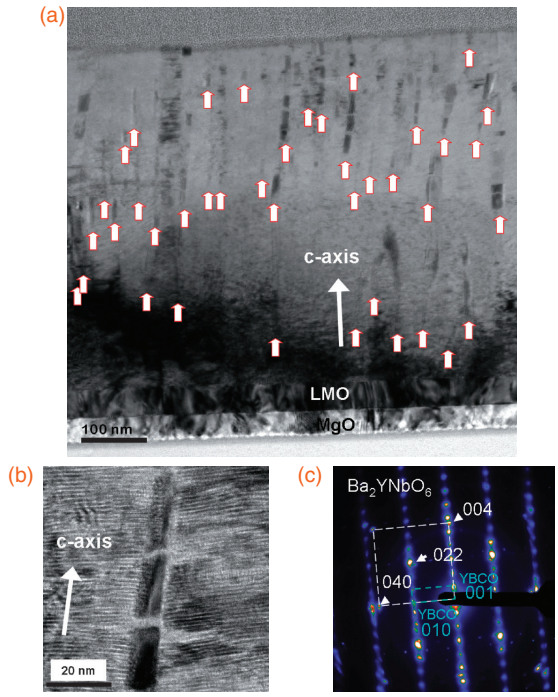

Fig. 1. Transmission electron micrographs of ~0.5-μm-thick YBCO film with 5.1% Ba_2YNbO_6 nanophase on IBAD-MgO templates. (a) Cross-section TEM image showing the presence of columnar defects comprised of self-assembled Ba_2YNbO_6 nanodots in general along the *c*-axis as indicated by arrows. (b) A higher magnification image showing a Ba_2YNbO_6 column comprised of a stack of nanorods. (c) Selected area diffraction (SAD) patterns taken from a cross-section TEM specimen indicating the presence of cubic, double perovskite Ba_2YNbO_6 nanocolumns.

to approximately 500–1000 μm^{-2}, which corresponds to matching field, B_ϕ, of 1–2 T. Despite the higher volume fraction of the BYNO nanophase in the YBCO matrix, this sample shows areal density and matching fields similar to those of YBCO films containing 1–2 vol % BZO.[14] This can be attributed to the nature of BYNO nanocolumns having nanorods with larger diameters and longer lengths, compared to BZO nanocolumns. Detailed morphological features of individual BYNO nanocolumns are shown in Fig. 1(b). The nanocolumn is composed of a stack of nanorods ~20 nm in length and 7–10 nm in diameter and has a very small gap of ~2–3 nm between the rods. Such morphology is in contrast to that observed in BZO nanocolumns comprised of nanodots in smaller diameters and shorter lengths.[5,14] Figure 1(c) shows selected area diffraction (SAD) pattern for the sample. Diffraction spots caused by the BYNO cubic perovskite structure are observed to be clearly distinguishable from those of the YBCO structure.

Figure 2 shows θ–2θ X-ray scans for YBCO films with and without BYNO nanocolumns. All samples exhibit a sharp

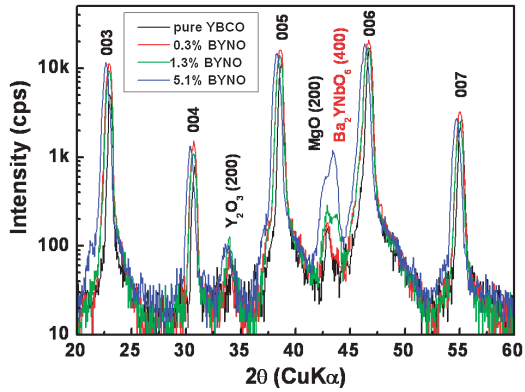

Fig. 2. θ–2θ X-ray diffraction results for YBCO films containing different % volume fractions of Ba_2YNbO_6 nanophase from 0 to 5.1%.

out-of-plane *c*-axis orientation with strong (00*l*) peak intensities of the YBCO phase. For YBCO+BYNO films, there is an additional peak at ~43.5° corresponding to BYNO (400) that provides direct evidence for the formation of an oriented BYNO nanophase within YBCO film. This peak also gets stronger with increasing BYNO volume fraction from 0.3 to 5.1%. Since Nb was only doped into YBCO film during the film growth, the BYNO nanophase is formed by the reaction between YBCO and Nb as represented as

$$YBa_2Cu_3O_{7-\delta} + xNbO_y \rightarrow (1-x)YBa_2Cu_3O_{7-\delta} + xBa_2YNbO_6 + 3xCuO.$$

Excess CuO phase forms in this reaction. However, CuO phase was not detected from θ–2θ scans for YBCO+BYNO films. Plan-view SEM examination shows 100–200 nm sized particles on the surface of YBCO+BYNO samples, which were not observed in pure YBCO film and likely correspond to this excess CuO (image not shown here). Some of the excess CuO is also expected to have been incorporated as 124-type stacking faults within YBCO. The ω- and φ-scans of the YBCO and BYNO phases in the YBCO+5.1% BYNO film were also measured (not shown here). Small values of full width half maximum (FWHM) of φ and ω scans ($\Delta\varphi_{(113)} \sim 3.52°$ and $\Delta\omega_{(006)} \sim 1.38°$) for the YBCO phase indicate excellent cube-on-cube epitaxy of the YBCO film. Although the BYNO nanophase ($\Delta\varphi_{(220)} \sim 5.47°$ and $\Delta\omega_{(400)} \sim 1.98°$) has larger $\Delta\varphi$ and $\Delta\omega$ than the YBCO film, X-ray results clearly indicate the epitaxial nature of the BYNO nanocolumns within the YBCO film with a crystallographic relationship corresponding to $[00l]_{BYNO} \parallel [001]_{YBCO}$.

YBCO+BYNO films show excellent superconducting properties. The samples with BYNO volume fraction from 0.3 to 5.1% have T_c of 87.4–88.3 K which is essentially unchanged compared to the undoped sample with a T_c of 87.6 K. The film with 1.3% BYNO nanocolumns was measured to have a self-field J_c of 4.1 MA/cm^2 at 77 K, significantly larger than the J_c of 2.8 MA/cm^2 for pure YBCO. Field and angular J_c performance is also remarkably improved via incorporation of BYNO nanocolumns, as shown in Fig. 3. Field dependent J_c for $H \parallel c$ in Fig. 3(a) shows that the 1.3 and 5.1% BYNO doped samples have 1.5–7 fold higher J_c in entire magnetic field regime up to 8 T (the highest field at which measurements were made), compared to the pure YBCO film. As shown in the inset of Fig. 3(a), α, the exponent in the power-law of $J_c \sim H^{-\alpha}$, is

© 2010 The Japan Society of Applied Physics

Person-to-person distribution (up to 10 persons) by the author only. Not permitted for publication for institutional repositories or on personal Web sites.

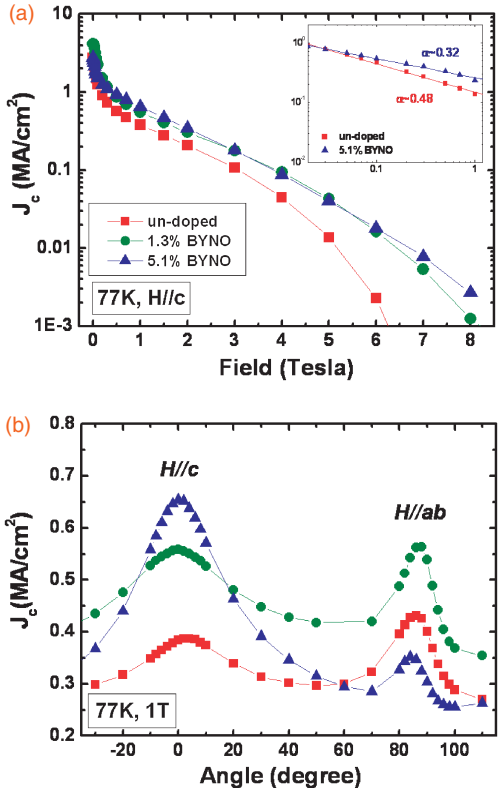

Fig. 3. The field dependent J_c at 77 K, $H \parallel c$ with the magnetic field up to 8 T (a) and the angular dependent J_c at 77 K, 1 T (b) for undoped, 1.3%-, and 5.1%-doped YBCO films.

also greatly reduced from ~0.48 for undoped sample to ~0.32 for 5.1% BYNO-doped film, indicating *c*-axis correlated pinning by BYNO columns. The irreversibility field, H_{irr}, at 77 K is also increased from ~6.3 T (undoped) to ~8 T (1.3% BYNO) and over 8 T for the 5.1% BYNO-doped film. Figure 3(b) shows the angular dependence of J_c at 77 K, 1 T. Compared to the undoped sample, the 1.3% BYNO-doped sample has a higher overall J_c in entire angular range. For the 5.1% BYNO-doped sample, much higher J_c and a stronger peak of J_c at $H \parallel c$ is observed. However, the J_c appears to be suppressed for the magnetic field orientation away from the *c*-axis toward the *ab*-planes. Such an angular J_c behavior is attributed to the increased density of BYNO nanocolumns which sufficiently perturbs the intrinsic pinning from the *ab*-planes, while strongly enhancing the *c*-axis correlated pinning. Such effects have been also reported from REBCO films containing a high density of BZO nanocolumns.[8)]

Formation of columnar defects comprised of Er-substituted $BaNbO_3$ cubic perovskite, which has a similar lattice constant with $Ba(Er_{0.5}Nb_{0.5})O_6$ phase was reported for ~0.3 μm thick, epitaxial films deposited on $SrTiO_3$ substrates using pulsed laser deposition from a target comprised of a mixture of $ErBa_2Cu_3O_x + BaNb_2O_6$.[19,20)] However, in these reports, the performance of the superconducting film was poor, with the maximum self-field J_c of such doped films being 0.2–0.5 MA/cm^2 at 77 K, self-field. In contrast, our films (0.65 μm) have columnar defects of the double perovskite, Ba_2YNbO_6 phase within the epitaxially grown YBCO film. Moreover, these thicker films have a high self-field J_c at 77 K of 4.1 MA/cm^2, with significantly improved in-field performance.

In conclusion, Ba_2RENbO_6 materials with cubic, double perovskite structure are suggested as a new class of additives resulting in superior flux-pinning and J_c of REBCO films. Epitaxial growth of the *c*-axis oriented, self-assembled BYNO nanocolumns within YBCO films deposited on IBAD-MgO metallic coated conductor templates was demonstrated. YBCO films having such BYNO nanocolumns have remarkably improved flux-pinning and consequently higher J_c over extensive field and angular ranges by a factor of 1.5–7 compared to YBCO film. No T_c reduction was also observed up to 5.1% BYNO volume fraction.

Acknowledgments We would like to thank SuperPower Inc. for providing the Hastelloy substrates with the multilayer configuration of IBAD MgO layer/Homoepitaxial MgO layer/Epitaxial $LaMnO_3$. This research was sponsored by the U.S. DOE Office of Electricity Delivery and Energy Reliability—Advanced Cables and Conductors under contract DE-AC05-00OR22725 with UT-Battelle, LLC managing contractor for Oak Ridge National Laboratory. This manuscript has been authored by UT-Battelle, LLC, under Contract No. DE-AC05-00OR22725 with the U.S. Department of Energy. The United States Government retains and the publisher, by accepting the article for publication, acknowledges that the United States Government retains a non-exclusive, paid-up, irrevocable, world-wide license to publish or reproduce the published form of this manuscript, or allow others to do so, for United States Government purposes.

1) *Second Generation HTS Conductors*, ed. A. Goyal (Kluwer Academic, Boston, MA, 2005).
2) T. Haugen, P. N. Barnes, R. Wheeler, F. Meisenkothen, and M. Sumption: Nature **430** (2004) 867.
3) K. Matsumoto, T. Horide, A. Ichinose, S. Horii, Y. Yoshida, and M. Mukaida: Jpn. J. Appl. Phys. **44** (2005) L246.
4) J. L. Macmanus-Driscoll, S. R. Foltyn, Q. X. Jia, H. Wang, A. Serquis, L. Civale, B. Maiorov, M. E. Hawley, M. P. Maley, and D. E. Peterson: Nat. Mater. **3** (2004) 439.
5) A. Goyal, S. Kang, K. J. Leonard, P. M. Martin, A. A. Gapud, M. Varela, M. Paranthaman, A. O. Ijaduola, E. D. Specht, J. R. Thomson, D. K. Christen, S. J. Pennycook, and F. A. List: Supercond. Sci. Technol. **18** (2005) 1533.
6) S. H. Wee, A. Goyal, P. M. Martin, M. Paranthaman, and L. Heatherly: Supercond. Sci. Technol. **19** (2006) L42.
7) S. Kang, A. Goyal, J. Li, A. A. Gapud, P. M. Martin, L. Heatherly, J. R. Thompson, D. K. Christen, F. A. List, M. Paranthaman, and D. F. Lee: Science **311** (2006) 1911.
8) S. H. Wee, A. Goyal, J. Li, Y. L. Zuev, and S. Cook: J. Appl. Phys. **102** (2007) 063906.
9) P. Mele, K. Matsumoto, A. Ichinose, M. Mukaida, Y. Yoshida, S. Horii, and R. Kita: Supercond. Sci. Technol. **21** (2008) 125017.
10) S. H. Wee, A. Goyal, Y. L. Zuev, and C. Cantoni: Supercond. Sci. Technol. **21** (2008) 092001.
11) S. H. Wee, A. Goyal, Y. L. Zuev, and C. Cantoni: Appl. Phys. Express **1** (2008) 111702.
12) Y. L. Zuev, D. Christian, S. H. Wee, A. Goyal, and S. W. Cook: Appl. Phys. Lett. **93** (2008) 172512.
13) S. H. Wee, A. Goyal, E. D. Specht, C. Cantoni, Y. L. Zuev, V. Selvamanickam, and S. Cook: submitted to Phys. Rev. B.
14) A. Goyal, S. H. Wee, C. Cantoni, Y. L. Zuev, E. D. Specht, J. Shin, Y. Gao, S. Cook, O. Polat, T. Aytug, K. Kim, J. Sinclair, J. R. Thompson, M. P. Paranthaman, and D. K. Christen: presented at 2009 Annual Peer Review for the U.S. Superconductivity Program for Electric Systems, August 4–6, 2009, Washington, D.C. (in preparation for publication).
15) K. Henmi and Y. Hiantsu: J. Solid State Chem. **148** (1999) 353.
16) J. Koshy, J. Kurian, J. K. Thomas, Y. P. Yadava, and A. D. Damdaran: Jpn. J. Appl. Phys. **33** (1994) 117.
17) C. G. S. Pillai and A. M. George: J. Mater. Sci. Lett. **11** (1992) 1639.
18) C. Greaves and P. R. Slater: Physica C **161** (1989) 245.
19) H. Kai, M. Mukaida, R. Teranishi, N. Mori, K. Yamada, S. Horii, A. Ichinose, R. Kita, K. Matsumoto, Y. Yoshida, S. Awaji, K. Watanabe, M. Namba, and T. Fujiyoshi: Physica C **468** (2008) 1854.
20) K. Yamada, M. Mukaida, H. Kai, R. Teranishi, A. Ichinose, R. Kita, S. Kato, S. Horii, Y. Yoshida, K. Matsumoto, and S. Toh: Appl. Phys. Lett. **92** (2008) 112503.

© 2010 The Japan Society of Applied Physics